Superoxide Reduction Mechanism of *Archaeoglobus fulgidus* One-Iron Superoxide Reductase†

João V. Rodrigues,‡ Isabel A. Abreu,§,|| Diane Cabelli,§ and Miguel Teixeira*,‡

Instituto de Tecnologia Química e Biológica, Universidade Nova de Lisboa, Av. da República (EAN), 2784-505 Oeiras, Portugal, and Chemistry Department, Brookhaven National Laboratory, Upton, New York 11973-5000

Received December 6, 2005; Revised Manuscript Received June 1, 2006

ABSTRACT: Superoxide reductases (SORs), iron-centered enzymes responsible for reducing superoxide (O_2^-) to hydrogen peroxide, are found in many anaerobic and microaerophilic prokaryotes. The rapid reaction with an exogenous electron donor renders the reductase activity catalytic. Here, we demonstrate using pulse radiolysis that the initial reaction between O_2^- and *Archaeoglobus fulgidus* neelaredoxin, a one-iron SOR, leads to a short-lived transient that immediately disappears to yield a solvent-bound ferric species in acid−base equilibrium. Through comparison of wild-type neelaredoxin with mutants lacking the ferric ion coordinating glutamate, we demonstrate that the remaining step is related to the final coordination of this ligand to the oxidized metal center and kinetically characterize it for the first time, by pulse radiolysis and stopped-flow kinetics. The way exogenous phosphate perturbs the kinetics of superoxide reduction by neelaredoxin and mutant proteins was also investigated.

Superoxide (O_2^-) is a known toxic byproduct of noncontrolled and incomplete oxygen reduction, in aerobes and in anaerobes transiently exposed to oxygen. A group of metal-centered enzymes, superoxide dismutases (SODs),[1] has evolved in living cells for the purpose of removing O_2^- via the alternate reduction and oxidation of the metal and concomitant production of oxygen and hydrogen peroxide (*1*−*3*).

$$M^{n+} + O_2^- \rightarrow M^{(n-1)+} + O_2 \quad (1)$$

$$M^{(n-1)+} + O_2^- + 2H^+ \rightarrow M^{n+} + H_2O_2 \quad (2)$$

In the past decade, a new class of iron-centered proteins has been shown to remove O_2^- via the reductive pathway (reaction 2) alone, and these enzymes are now called superoxide reductases (SORs) (*4*−*15*). As shown in reaction 2, a superoxide reductase donates one electron and potentially two protons to the superoxide to produce hydrogen peroxide. SORs have thus far been found only in anaerobic and microaerophilic prokaryotes and constitute a system for antioxidant defense against the superoxide that can be formed upon transient exposure of the cells to oxygen. Moreover, many of these organisms rely solely on SORs to scavenge O_2^- as no canonical SODs are encoded in their genomes (of the 21 available SOR-containing genomes, 11 do not have SOD, as judged from a comprehensive survey of all complete genomes).

These proteins are found with either one iron center or two iron centers and are called neelaredoxin (Nlr) and desulfoferrodoxin (Dfx), respectively. The common iron center that is responsible for the reduction of O_2^- (center II) is composed of a pentacoordinated iron(II) with four equatorial histidines and one protein-buried axial cysteine in a square pyramidal geometry (*16*−*18*). A sixth, solvent-exposed, glutamate is coordinated in the other axial position of the oxidized metal site, resulting in an octahedral geometry (*16*). That axial site is vacant when the metal is reduced, and it is likely the site of O_2^- binding. Desulfoferrodoxin has an additional desulforedoxin-like iron center (center I) that consists of iron tetrahedrally coordinated to four cysteines (*18*).

It has been shown by pulse radiolysis studies that neelaredoxin from the hyperthermophilic archaeon, *Archaeoglobus fulgidus*, operates by a virtually diffusion-controlled superoxide reductase (reaction 2) pathway (*6*). Similar studies performed with Dfx from *Desulfovibrio vulgaris* and *Desulfoarculus baarsi* and Nlr from *Treponema pallidum* showed the same rates of reduction of O_2^- (*9*, *11*, *19*). The role of the desulforedoxin-like iron center in the kinetic process of O_2^- reduction was addressed previously by selective mutation of iron-binding cysteines to produce an enzyme that could not bind iron in that site. No difference was found in the activity of an enzyme with both iron centers and that of the enzyme lacking the desulforedoxin-like center (*13*).

† This work was financed by FCT (Portugal) Project POCTI/BME/37406/2002 and Grant SFRH/BD/14380/2003 to J.V.R.

* To whom correspondence should be addressed: Instituto de Tecnologia Química e Biológica, Universidade Nova de Lisboa, Av. da República (EAN), 2784-505 Oeiras, Portugal. Phone: 351 21 4469322. Fax: 351 21 4469314. E-mail: miguel@itqb.unl.pt.

‡ Universidade Nova de Lisboa.

§ Brookhaven National Laboratory.

|| Present address: Laboratory of Plant Molecular Biology, Rockefeller University, 1230 York Ave., New York, NY 10021.

[1] Abbreviations: SOR, superoxide reductase; SOD, superoxide dismutase; Nlr, neelaredoxin; Dfx, desulfoferrodoxin; Rd, rubredoxin.

10.1021/bi052489k CCC: $33.50
Published on Web 07/08/2006

The superoxide reduction by SOR has been proposed to proceed by the formation of a transient species exhibiting an absorption maximum at 590−600 nm ($\epsilon \sim 3000-4000$ M^{-1} cm^{-1}), which is generally assigned to a ferric hydroperoxo species (*6*, *7*, *9*−*11*, *14*, *15*). The nature of this short-lived intermediate was characterized by computational studies on the active site that suggested that end-on peroxo/hydroperoxo ferric species were stable, in contrast with a side-on peroxo species that resulted in dissociation of iron−imidazole bonds (*20*). Somewhat opposing results were obtained in studies on mutants of *D. baarsi* and *T. pallidum* SORs without the glutamate ligand, where a stabilized side-on Fe^{3+}−peroxo species was trapped upon incubation with hydrogen peroxide (*21*, 22). The spectrum of the resulting species has an absorption maximum at 560 nm and an extinction coefficient of <1000 M^{-1} cm^{-1}, somewhat different from that of the intermediate observed in pulse radiolysis studies for the same enzymes (∼600 nm, $\epsilon \sim 3000$ M^{-1} cm^{-1}) (*11*, *14*). Therefore, it is not clear if these two species are the same. In the case of a biomimetic model of SOR, $\{Fe^{2+}[S^{Met}N_4(tren)]\}^+$, formation of a hydroperoxo intermediate upon reaction with O_2^- was reported (*23*). Moreover, the oxidation of this compound by O_2^- in organic media takes place only in the presence of a proton source (*24*), showing that the initial step of O_2^- reduction is tightly coupled with proton transfer in this system. With the SOR enzymes, if the initial reaction with O_2^- involves a proton transfer, it should be nonlimiting, since the corresponding rate constant is pH-independent and no significant isotope effect was observed (*10*, *14*).

Conflicting results were reported with regard to the process of decay of the first intermediate formed in SORs. In both *A. fulgidus* Nlr and *D. vulgaris* Dfx, this intermediate appears to decay by a first-order process, ending in the "resting" oxidized enzyme (*7*, *10*), while in *D. baarsi* Dfx, a better data fit is obtained by the sum of two first-order processes (*14*). Nevertheless, this decay seems to involve a rate-limiting protonation, as judged by the pH-dependent profile and isotope effect, corresponding to one of the protons needed for the reaction (*10*, *14*). The glutamate ligand was first proposed to promote H_2O_2 release of the center; however, mutation of this residue does not directly alter the kinetics of O_2^- reduction at physiological pH (*7*, *10*, *14*). Glutamate presumably binds upon oxidation of the iron center by O_2^-, but this process has not yet been characterized kinetically.

The catalytic cycle for the reduction of O_2^- by SOR is completed after the re-reduction of the oxidized iron center by external electron donors. It was shown that rubredoxins, small non-heme iron proteins, can efficiently transfer electrons to *A. fulgidus* neelaredoxin ($k = 10^7$ M^{-1} s^{-1}) (*25*) and *D. vulgaris* desulfoferrodoxin ($k = 10^6$ M^{-1} s^{-1}) (*13*), these being the most likely redox partners of SORs.

Here, we reevaluate the kinetics of O_2^- reduction by *A. fulgidus* Nlr and mutants where the glutamate is replaced with a valine (E12V Nlr) or a glutamine (E12Q Nlr) in an effort to define the role of the glutamate ligand. In addition, we have examined the entire reductase mechanism in the presence and absence of phosphate to ascertain whether phosphate binding has led to complications in explaining the overall mechanism of O_2^- reduction.

EXPERIMENTAL PROCEDURES

Expression and Purification of Recombinant Neelaredoxin and Mutants. *Escherichia coli* cells harboring plasmids pT7AfNlr, pT7AfNlrE12Q, and pT7AfNlrE12V (*7*, *26*) were grown aerobically at 25 °C in M9 minimal medium supplemented with 100 μg/mL ampicillin and 10 μM $FeSO_4$ in a 10 L fermentor. When the culture reached a cell density at which A_{600} equaled 0.3, 0.5 mM isopropyl 1-thio-β-D-galactopyranoside was added, and the cells were harvested by centrifugation (10000*g* for 10 min) after 6 h and washed with 10 mM Tris-HCl (pH 7.2). All subsequent purification steps were performed at 4 °C. The cells were broken in a mini-cell French press at 900 psi. After ultracentrifugation (100000*g* for 4 h), the soluble extract was dialyzed against 10 mM Tris-HCl (pH 7.2) and loaded in a Q-Sepharose column (Pharmacia) previously equilibrated with the same buffer. A linear gradient from 0 to 0.5 M NaCl was applied, and the fractions containing Nlr were eluted at 0.25 M NaCl. This fraction was dialyzed against 10 mM Tris-HCl (pH 7.2) and loaded in a Fractogel EMD TMAE column (Merck) equilibrated with the same buffer. A linear gradient from 0 to 0.5 M NaCl was applied, and the fraction containing Nlr was eluted at 0.25 M NaCl. The sample was concentrated by ultrafiltration and loaded in a Superdex 75 column (Pharmacia) equilibrated with 20 mM Tris-HCl (pH 7.2) and 150 mM NaCl. Protein purity was tested by SDS−PAGE, and the bicinchoninic acid protein assay kit (Pierce) (*27*) was used to determine the protein concentration. The total iron content was determined by the 2,4,6-tripyridyl-*s*-triazine (TPTZ) method (*28*).

Spectroscopic Studies. Fully oxidized proteins were obtained by incubation with excess potassium hexachloroiridate (K_2IrCl_6) (Sigma) followed by ultrafiltration for the removal of excess oxidant. Room-temperature UV−visible spectra were recorded on a Shimadzu UV-1603 spectrophotometer. The extinction coefficients of the oxidized proteins were calculated by oxidizing the ascorbate-reduced proteins (∼80 μM) with superoxide radical (∼7 μM) generated by irradiating an air-saturated solution containing 10 mM formate in a ^{60}Co source (0.69 μM superoxide produced per second of incubation) for set time periods. The changes in absorbance were plotted against the total concentration of superoxide added, and the extinction coefficients were then calculated by the slope in the early linear region. Alternatively, K_2IrCl_6 was used as an oxidant, where the concentration of K_2IrCl_6 was determined by successive additions of this oxidant to a solution of reduced horse heart cytochrome *c* (Sigma) and measurement of the absorbance decrease at 550 nm ($\epsilon_{\text{cytochrome } c} = 21\,500$ M^{-1} cm^{-1}), yielding an extinction coefficient for K_2IrCl_6 ($\epsilon_{488} = 5000$ M^{-1} cm^{-1}). EPR spectra were recorded on a Brucker EMX apparatus equipped with a continuous flow Oxford Instruments helium cryostat.

NADH:Superoxide Oxidoreductase Activity. The NADH:superoxide oxidoreductase assay was performed as described by Emerson et al. (*13*) with some modifications. Reaction mixtures contained 20 mM Tris-HCl (pH 7.6), 10% glycerol, 60 μM NADH, 170 units/mL catalase, 200 μM xanthine, 1.6 μM *A. fulgidus* rubredoxin AF1349, 3 μM Nlr, and 60 nM *E. coli* NADH:flavorubredoxin oxidoreductase (*29*) which efficiently catalyzes the reduction of rubredoxin by NADH (*25*). The background NADH consumption rate was

measured prior to the addition of xanthine oxidase. The superoxide fluxes, in the range of 1−10 μM/min, were calibrated by measuring the rate of horse heart cytochrome *c* reduction. The consumption of NADH was assessed by the decrease in absorbance at 340 nm (ϵ_{340} = 6.2 mM^{-1} cm^{-1}).

pH Studies. The changes in the absorbance spectrum of each protein (final concentration of 20−40 μM) were studied in the range of pH 4.5−11 by diluting samples from a concentrated stock of fully oxidized protein in buffer mixtures containing formate, 2-(*N*-morpholino)ethanesulfonic acid (MES), Tris-HCl, bis-tris propane, and glycine (50 mM each) at a desired pH. Alternatively, the titration was carried out with a low-buffered protein solution (each buffer component at 2−5 mM), and small additions of HCl or NaOH were used to change the pH while spectra were successively recorded.

Pulse Radiolysis Studies. Pulse radiolysis experiments were carried out using the Brookhaven National Laboratory (BNL) 2 MeV Van de Graaff accelerator as described previously (*30*). $(SCN)_2^-$ provided dosimetry assuming a *G* value of 6.00 and a molar extinction coefficient of 7950 M^{-1} cm^{-1} at 472 nm. Superoxide radicals (1−20 μM) were generated using doses of 100−2500 rads. Water radiolysis yields the following radicals and/or molecular products, where the numbers in parentheses are *G* values, which is the number of molecules per 100 eV of energy absorbed by the medium (*31*)

$$H_2O \rightarrow e_{aq}^- (2.75), {}^\bullet OH (2.65), H (0.65), H_2O_2 (0.7), H_2 (0.45) \quad (3)$$

The primary radicals e_{aq}^-, $^\bullet$OH, and H can be converted to O_2^- radicals with the addition of formate (HCO_2^-) and oxygen (*32*)

$$e_{aq}^- + O_2 \rightarrow O_2^{\bullet -} \quad pK(HO_2/O_2^{\bullet -}) = 4.8 \quad (4)$$

$$^\bullet OH/H + HCO_2^- \rightarrow H_2O/H_2 + CO_2^{\bullet -} \quad (5)$$

$$CO_2^{\bullet -} + O_2 \rightarrow O_2^{\bullet -} + CO_2 \quad (6)$$

All pulse radiolysis samples were prepared using Millipore ultrapurified distilled water. Ethylenediamminetetraacetate (EDTA), sodium formate, ethanol, monobasic phosphate, sodium hydroxide, and hydrochloric acid were of the highest purity commercially available and used as purchased. Reduced enzyme was obtained by addition of stoichiometric quantities of ascorbate to a solution of Nlr. Unless otherwise mentioned, most studies were performed at room temperature in air-saturated solutions containing 10−100 μM SOR sites, 2 mM Tris-HCl, 5 mM NaCl, and 5 mM formate and were pulsed with doses of 1.1−3.6 μM O_2^-. Alternatively, 0.5 M ethanol was used as a $^\bullet$OH scavenger instead of formate (*33*). The quantitative formation of the superoxide radical was observed prior to its reaction with the SOR, verifying that release of superoxide was fast, using either radical scavenger. The data were analyzed using the BNL Pulse Radiolysis Program.

Stopped-Flow Experiments. The rapid kinetics of oxidation of Nlr by K_2IrCl_6 were determined at room temperature, using a Bio-Logic stopped-flow SM400/S apparatus equipped with a MOS-200 optical system. Reduced Nlr was obtained by incubation with excess ascorbate, followed by utrafiltration to remove the reductant. Solutions (60 μM) of reduced Nlr and K_2IrCl_6 (70 μM), both prepared in 5 mM Tris-HCl (pH 7.6), were loaded in two separate drive syringes, and after the stopped-flow mixing had been carried out (1:1, v/v), the absorbance changes were monitored at wavelengths between 470 and 730 nm. As no further absorbance changes were observed beyond 300 ms, the UV−vis spectrum of the protein sample was used to correct the values of the final absorbance determined by stopped-flow experiments at each wavelength. For pH studies, 5 mM MES or bis-tris-propane was used for buffering in the pH range of 5−9. The data were analyzed using Biokine version 3.29.

Phosphate Binding Studies. The changes in absorbance at 613 nm of E12V neelaredoxin (64 μM) in 5 mM Tris-HCl, 5 mM MES, and 0.1 M NaCl at pH 6.5 were recorded after successive additions of potassium phosphate (from 0.1 to 94 mM) to the fully oxidized protein. The dissociation constant (K_D) was determined by fitting the expression $P_{bound} = 1/(1 + K_D/P)$ to the data, where P_{bound} is the fraction of enzyme with phosphate bound and *P* is the free phosphate concentration.

RESULTS

Recombinant *A. fulgidus* neelaredoxin is isolated mainly as a homotetramer, as determined by gel filtration chromatography, although smaller amounts of higher oligomeric states are also formed. For this work, only the most abundant tetrameric form was used. Interestingly, no significant amounts of oligomeric forms higher than the tetramer were formed for the E12V Nlr and E12Q Nlr mutants. The iron content of purified Nlr yielded 0.8 iron atom per monomer, where this ratio was 1.2 and 0.9 for E12V and E12Q mutants, respectively. As reported previously, the EPR spectra of the oxidized wild-type enzyme and both mutants exhibit g = 7.2 and 5.8 resonances characteristic of a high-spin ($S = {}^5/_2$) species with an axial distortion ($E/D \approx 0.06$) and a g = 4.3 resonance characteristic of a high-spin ($S = {}^5/_2$) species with rhombic symmetry ($E/D = 0.33$) (*7*; data not shown). This rhombic species arises from adventitiously bound Fe^{3+} which does not contribute to the visible spectra of these proteins, and it is not reduced by ascorbate [shown for the one-Fe SOR of *Pyrococcus furiosus* and *T. pallidum* (*8*, *34*)]. The extinction coefficients of the visible absorbing iron species were determined by measuring the increase in absorbance upon oxidation by superoxide (see Experimental Procedures), and assuming that each superoxide radical oxidizes one iron center. Similar results were obtained using hexachloroiridate(IV) as an oxidant. The fraction of optically absorbing iron, of the total iron content, is 83% for wild-type Nlr, 80% for E12V, and 74% for E12Q. The extinction coefficients used in this work are based on the active iron content.

NADH:Superoxide Oxidoreductase Activity. A pathway for reduction of superoxide by NADH using NADH:rubredoxin oxidoreductase, rubredoxin, and Nlr was reconstructed. Using calibrated superoxide fluxes produced by the xanthine/xanthine oxidase system, the rate of consumption of NADH by this pathway was studied in the same manner that was described previously (*13*). We found that the rate for NADH

oxidation was proportional to that of superoxide production (1−10 μM superoxide flux) and the stoichiometry was 0.5 ± 0.1 NADH oxidized for each superoxide produced (not shown). Negligible NADH consumption rates above background were observed if either protein component of the pathway was absent from the reaction mixture. These results clearly show that one electron is consumed by each superoxide molecule, which corroborates the assumption made above for the calculation of the extinction coefficients and indicates that H_2O_2 is the natural product of the reaction.

Acid−Base Equilibria in Oxidized Neelaredoxins. The characteristic blue absorbance bands of wild-type Nlr and both E12V and E12Q mutants were studied as a function of pH. In all cases, a fully reversible shift of the wavelength of the absorbance maximum was observed when the pH was changed, and this dependence could be adjusted with a single proton dissociation equilibrium curve (Figure 1). It should be noted that the reversibility refers only to the effect on the electronic properties of the iron site, as at extreme pH values the protein is not very stable. The pK_a of this spectral shift is 9.6 ± 0.2 for wild-type Nlr (Figure 1A), whereas in the E12V mutant, the pK_a is lowered to 6.3 ± 0.2 (Figure 1B). The spectra of the E12Q mutant were identical to those of E12V, and the measured pK_a was 6.8 ± 0.2 (not shown). It was recently shown that the origin of this pK_a is hydroxide binding at high pH, replacing the glutamate ligand (*35*). At low pH, a water molecule most probably coordinates the iron center of the mutants. The lower pK_a determined for the mutants is consistent with this in that, in the absence of the glutamate ligand, the hydroxide does not have to compete with the glutamate to bind to the iron center. As shown in Figure 1, the major consequence of the glutamate mutation on the visible spectra of the low-pH species is a change in the extinction coefficient, which is ∼700 M^{-1} cm^{-1} lower in the mutants, while the maximum wavelength is roughly the same for Nlr and both mutants (666 and 670 nm, respectively). In contrast, the spectral band of the high-pH species is similar for Nlr and the two mutants in which glutamate is replaced, with an absorption maximum at ∼590 nm and an extinction coefficient of approximately 2700 M^{-1} cm^{-1}. This similarity is again consistent with hydroxide binding at alkaline pH for both Nlr and the glutamate mutants.

Phosphate and Fluoride Binding. The spectra of E12V and E12Q mutants are significantly altered in the presence of phosphate (in the millimolar range, Figure 1C). The 590 nm band observed at pH 7.5 is shifted, in the presence of phosphate, to 620 nm, and its extinction coefficient is increased to ∼3000 M^{-1} cm^{-1}. The appearance of this new 620 nm species can be fitted by a one-binding site saturation curve, with a dissociation constant for phosphate (K_D) of 3.6 ± 0.1 mM at pH 6.5 (Supporting Information). The band of this 620 nm species also undergoes a blue shift with an increase in pH, and the same characteristic high-pH species, with a maximum at 590 nm, is observed at alkaline pH. The measured pK_a for this pH dependence is 9.0 ± 0.3 (for both mutants), a value very close to the pK_a of the wild-type protein. Here, phosphate is preventing binding of hydroxide in a fashion similar to that of glutamate in the wild-type protein, resulting in an increase in the pK_a.

No change in the spectrum or the pK_a is observed if phosphate is added to the wild-type protein (Figure 1A, inset). This suggests that phosphate binds to the iron vacant site in the mutants, but in the wild-type protein, the glutamate prevents binding of the phosphate. A summary of these results is presented in Scheme 1.

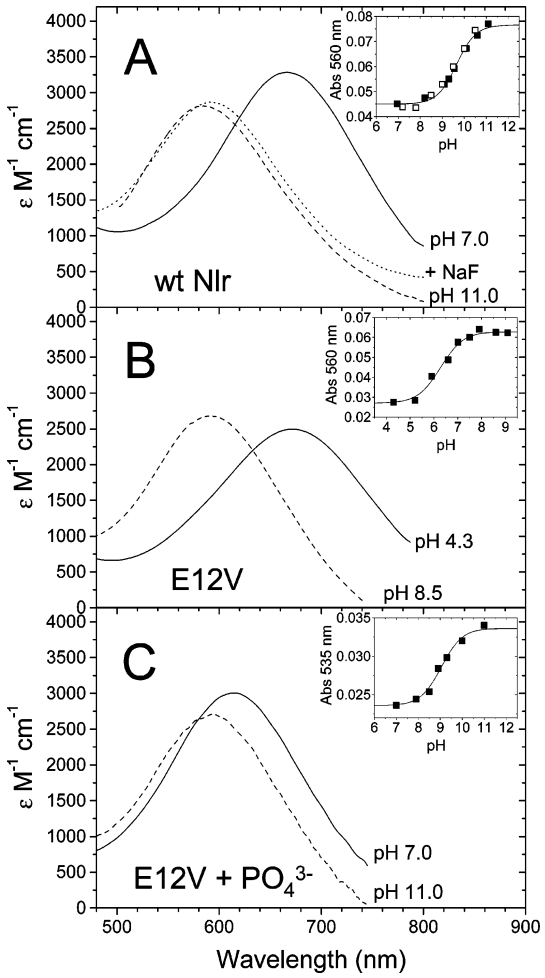

FIGURE 1: pH dependence of the visible absorption spectra of neelaredoxin (A) and the E12V mutant in the absence (B) or presence (C) of 50 mM potassium phosphate. The proteins (20−30 μM) were treated with K_2IrCl_6, and spectra recorded at low (—) and high pH (- - -) and in the presence of 30 mM NaF (•••, neelaredoxin only). Extinction coefficients at a given pH were determined by the changes in absorbance upon oxidation by controlled amounts of superoxide produced by irradiation of air-saturated protein solutions in a ^{60}Co source in the presence of 0.5 M ethanol. Insets show the pH dependence of the absorbance at a given wavelength, and the solid lines were obtained assuming a single protonation equilibrium, with pK_a values of 9.6 (A), 6.3 (B), and 9.0 (C). White squares in the inset of panel A are data obtained in the presence of 20 mM phosphate.

Scheme 1: Summary of pH-Dependent Equilibria Occurring in wt Nlr and E12 Mutants

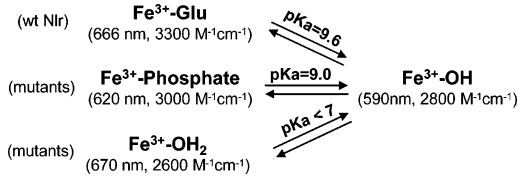

Fluoride was also investigated in this work as a potential ligand to the active center of neelaredoxin, and the spectrum obtained after the addition of 30 mM NaF to the protein solution at pH 7.0 is presented in Figure 1A (dotted line).

Table 1: Rate Constants k_1-k_3 Obtained for the Two Transient Species Formed during the Reaction of SORs with Superoxide[a] at pH 7.0

	k_1 ($\times 10^{-9}$ M^{-1} s^{-1})	k_2 ($\times 10^{-2}$ s^{-1})	k_3 (s^{-1})
Nlr	1.2 ± 0.2	3.8 ± 0.3	25 ± 2
E12V	0.22 ± 0.04	3.6 ± 0.2	−
E12Q[b]	0.9 ± 0.2	6.6 ± 0.2	−

[a] Rates were determined from the time courses of absorbance changes at different wavelengths following pulse radiolysis at 25 °C, in air-saturated solutions, containing 50 μM SOR sites, 2 mM Tris-HCl, 5 mM NaCl, and 0.5 M ethanol, and pulsed with 1.1−3.6 μM O_2^-. Values were averaged from three to five determinations, and the 95% confidence error intervals are reported. [b] Measured at pH 8.0.

Interestingly, the resulting spectrum resembles that of the Fe^{3+}−OH form, and it is invariant in the pH range from 5.4 to 9.1, which again suggests that the blue-shift transition is due to binding of a small anionic ligand. The spectrum of the fluoride-incubated protein is similar for the wild type and both mutant proteins, which indicates that fluoride, unlike phosphate, is able to replace the glutamate ligand over the entire pH range that was studied.

Pulse Radiolysis Studies of Neelaredoxin. The reactivity of Nlr toward O_2^- was studied using pulse radiolysis. In these experiments, the protein, which is ∼50% oxidized after purification, was totally reduced with stoichiometric amounts of sodium ascorbate. The concentration of $Fe(His)_4(Cys)$ sites was typically in a 5−50-fold excess over the O_2^- concentration so pseudo-first-order conditions could be achieved. As previously reported, formation of a 620 nm species (T_1) is observed within 50 μs of the pulse with a first-order rate constant proportional to the protein concentration ($k_1 = 1.3 \times 10^9$ M^{-1} s^{-1}). The subsequent changes in absorbance can be described by two first-order processes, both occurring at rates independent of enzyme concentration. Table 1 lists the rate constants obtained for each process at pH 7.0, and the reconstituted spectrum of each transient species is shown in Figure 2A. The extinction coefficients reported for each transient were calculated assuming that each superoxide radical produced in a pulse reacts with one ferrous active site. The reconstituted spectrum of the final species can be superimposed with the spectrum of the K_2IrCl_6-oxidized enzyme at pH 7.2. This again corroborates that the stoichiometry of the reaction of reduced Nlr with superoxide is 1:1, involving transfer of a single electron yielding H_2O_2 as a final product. Moreover, the reaction of H_2O_2 with reduced or oxidized SOR is much slower than the processes observed in the pulse radiolysis experiments (not shown), which eliminates the possibility of H_2O_2 influencing the reaction on the time scale used here. The spectrum of the second transient (T_2) is very similar to that of the oxidized enzyme at pH 11, which has been convincingly attributed to the Fe^{3+}−OH state (*35*). This immediately suggests that upon reaction with O_2^- at pH 7, an initial transient involving both O_2^- and iron is formed. This disappears with the concomitant formation of the hydroxide-bound ferric species. The ferric species then equilibrates to the glutamate-bound species observed at pH 7. Moreover, the formation of the ferric−hydroxide species as the second transient implies that the reaction product, hydrogen peroxide, is formed by this stage and no longer bound to the center.

Pulse Radiolysis Studies of Neelaredoxin E12V and E12Q Mutants. The E12V and E12Q Nlr mutants were purified in the reduced form, so no ascorbate was needed as a reductant. Nevertheless, stoichiometric reduction with ascorbate was sometimes used on a sample of an enzyme that had been oxidized by O_2^-, and no differences were observed in the spectral features and kinetics parameters compared with those using the as isolated reduced protein. The reaction of each mutant Nlr with O_2^- led to the immediate formation of a transient species absorbing at 620 nm (T_1), similar to the one observed with wild-type Nlr, by a first-order rate that was again proportional to protein concentration. For E12Q, the calculated bimolecular rate constant is very close to that obtained for wild-type Nlr ($k = 0.9 \times 10^9$ M^{-1} s^{-1}), while for the E12V mutant, it is about 1 order of magnitude lower ($k = 2.2 \times 10^8$ M^{-1} s^{-1}).

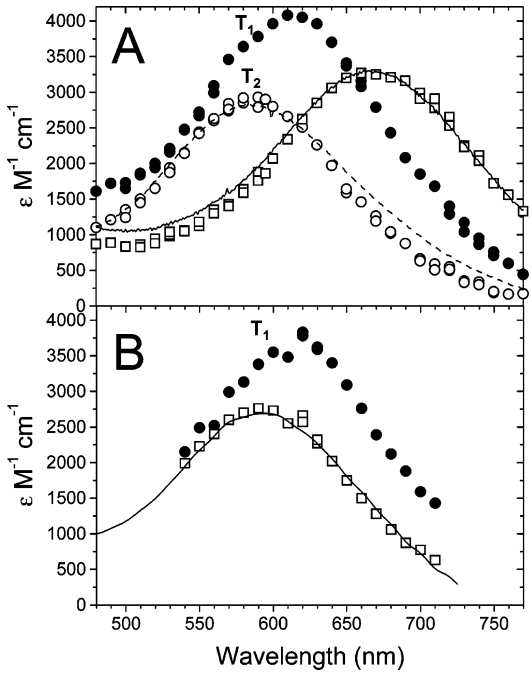

FIGURE 2: Transient absorption spectra formed upon reaction of (A) Nlr and (B) the E12V mutant with O_2^- at pH 7.5. Black circles depict the spectra of the initial transient (T_1), white circles those of the second transient (T_2, for only wt Nlr), and white squares those of the final product. Air-saturated solutions contained 50 μM SOR, 2 mM Tris-HCl, 5 mM NaCl, 0.5 M ethanol, and 1.1−3.6 μM O_2^-. The extinction coefficients were calculated assuming that each O_2^- reacts with one reduced iron. The solid lines are the absorption spectra of ferric states of the respective enzymes at pH 7.5, and the dashed line corresponds to the absorption spectrum of oxidized Nlr at pH 11.

The initial reaction with superoxide, and concomitant formation of T_1, was followed by a single first-order reaction leading to the formation of a species indistinguishable from the resting oxidized protein at that pH (Figure 2B).

Effect of pH on Transient Spectra and Rate Constants. The spectrum of the first intermediate (T_1) obtained upon reaction of reduced wt Nlr with O_2^- showed no significant changes in the pH range studied here. In contrast, the spectrum of the second transient (T_2) undergoes a pH-dependent shift with an associated pK_a of 6.1 ± 0.3 (Figure 3). The spectrum of protonated T_2 is similar to that of the low-pH Fe^{3+}−OH_2 species observed at low pH for the mutants (Figure 1B). Again, T_2 is best described as having an oxidized iron center with an unbound glutamate and an intrinsic pK_a of 6.1 and that the last step observed with Nlr,

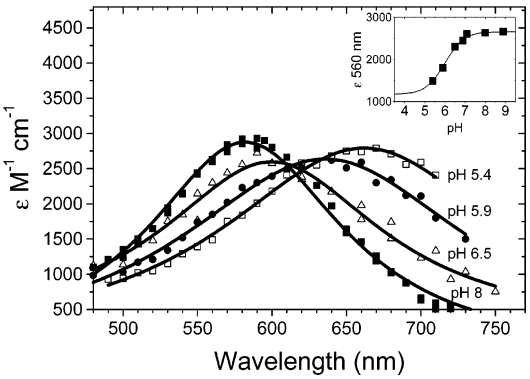

FIGURE 3: Reconstituted visible absorption spectra of T_2 observed in the reaction of wt Nlr with superoxide at pH 5.4, 5.9, 6.5, and 8. The inset shows the pH dependence of the extinction coefficient at 560 nm, and the solid line was obtained assuming a single protonation equilibrium, with a pK_a of 6.1.

Scheme 2: Processes Observed during the Reaction of Reduced Nlr with O_2•−

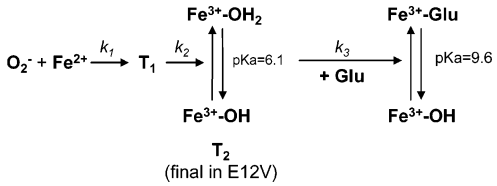

but not with the mutants, is the process of glutamate binding, leading to an increase in the pK_a from 6.1 to 9.6 as shown in Scheme 2 (see Discussion).

The pH dependences of the observed rates were studied over the pH range from 5.2 to 10 (it was not possible to go beyond these pH limits due to protein instability). The rate of formation of the initial transient, T_1, in both *A. fulgidus* Nlr and the E12V mutant shows little pH dependence (not shown), consistent with a process that does not involve a rate-limiting protonation. For wt Nlr, the rate of decay of T_1 (k_2) exhibits a significant decrease with an increase in pH up to ~7 followed by a plateau phase, and above pH ~8, it starts to increase (Figure 4A). This suggests the involvement of a rate-limiting protonation by H_3O^+ or a protein residue at low pH, unimolecular decomposition or water attack in the midphase, and a rate-limiting deprotonation or the binding of OH^- at high pH (see Discussion). In contrast to that of wild-type Nlr, the rate of decay of T_1 (k_2) in the E12V Nlr mutant is pH-independent in the pH range of 5.2−9, with a rate constant of 3.8×10^2 s^{-1}. The rate of decay of T_1 for the E12Q mutant is 2-fold higher than that of wt and E12V at pH 8. However, for both mutants, the rate exhibits little pH dependence down to pH 5.4 (not shown). At pH >9, the rate constant for the decay of T_1 (k_2) for the E12V mutant starts to increase with an increase in pH as observed for the wt protein.

The disappearance of the second transient (k_3), a process that is observed with only wt Nlr (as discussed previously), is also pH-dependent (Figure 4B) and slows with an increase in pH until it reaches a constant value at pH 8. If a single protonation equation is fitted to the data points, a pK_a of ≤6.3 is obtained (not shown), a value very similar to the pK_a calculated for the pH-induced spectral shift of T_2 that was assigned to the equilibrium between bound water and OH^-.

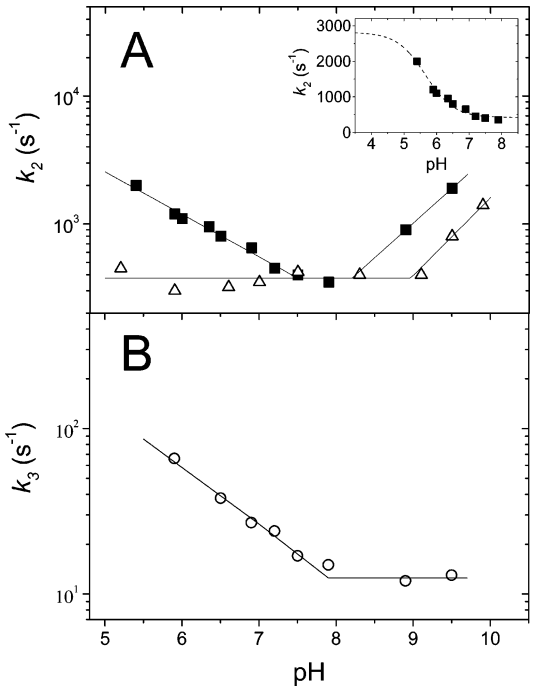

FIGURE 4: (A) pH dependence of the rate constant for the decay (k_2 in Scheme 2) of the first intermediate (T_1) formed upon reaction with superoxide obtained for Nlr (■) and the E12V Nlr mutant (△). The inset shows the data points obtained for wt Nlr fitted with a single-protonation equilibrium curve with a pK_a of 5.7 (—). (B) pH dependence of the rate constant for the decay (k_3 in Scheme 2) of the second intermediate (T_2) formed upon reaction with superoxide obtained for wt Nlr. Air-saturated solutions contained 50 μM SOR, 2 mM Tris-HCl, 5 mM NaCl, 5 mM formate, and 1.1−3.6 μM O_2^-. Values were averaged from three to five determinations.

Oxidation of Nlr by K_2IrCl_6. The oxidation of Nlr by K_2IrCl_6 was studied by stopped-flow spectrophotometry to compare the kinetics with those obtained in the aforementioned studies of the oxidation by O_2^-. Rapid mixing of 30 μM Nlr with 35 μM K_2IrCl_6 (final concentrations, pH 7.6) leads to immediate formation of an oxidized species with a spectrum almost identical to that of the high-pH form (Fe^{3+}−OH), which decays to the final product (Fe^{3+}−Glu species) with an apparent rate constant of 21 s^{-1} (Figure 5A). The initial oxidation by K_2IrCl_6 was too fast to be measured with our instrumentation, as it was completed within the 3.8 ms mixer dead time. The subsequent process was found to be independent of protein concentration with an observed rate that is very similar to k_3 measured in the reaction of reduced Nlr with O_2^-. The rate constant for the process after oxidation by K_2IrCl_6 is pH-dependent (Figure 5B). The data for this rate constant can be fitted by a single protonation equilibrium equation with an apparent pK_a of 6.0 ± 0.2. The spectrum of the initial species formed upon oxidation by K_2IrCl_6 is also pH-dependent, shifting toward blue with an increase in pH with an apparent pK_a of 6.2 ± 0.4 (Figure 5B, inset), revealing properties highly similar with those of the Fe^{3+}−OH/OH_2 species observed for the mutants and those of T_2 observed in the reaction of wt Nlr with O_2^-. Moreover, the pH dependence of the rate constant for the conversion to the final Fe^{3+}−Glu form is quite similar when either K_2IrCl_6 or O_2^- is used as the oxidant (k_3 is shown in Figure 5B for comparison). This is in agreement with the mechanism proposed in Scheme 2, in which T_2 is a solvent-bound oxidized Nlr that decays to an Fe^{3+}−Glu species.

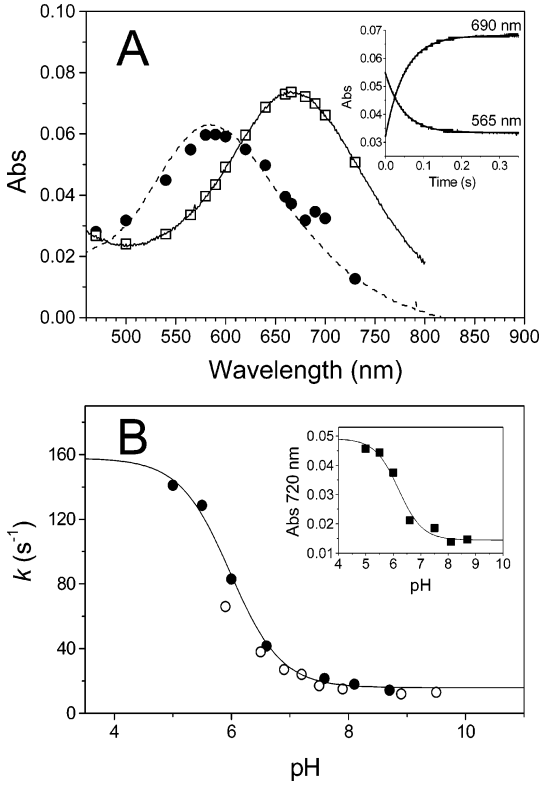

FIGURE 5: (A) Transient visible absorption spectra formed upon oxidation of wt Nlr by hexachloroiridate(IV) at pH 7.6. Black circles depict the spectra of the initial transient and white squares the spectra of the final product. The solid lines are the absorption spectra of the ferric state of the enzyme at pH 7.5, and the dashed line corresponds to the absorption spectrum of oxidized Nlr at pH 11. Solutions of 60 μM reduced Nlr and 70 μM K_2IrCl_6, prepared in 5 mM Tris-HCl (pH 7.6), were mixed (1:1, v/v). The inset shows the absorbance changes with time at 690 and 565 nm. (B) pH dependence of the rate of disappearance of the initial transient observed upon rapid mixing of reduced wt Nlr with hexachloroiridate(IV) (●). The solid line assumes a single protonation equilibrium, with a pK_a of 6.0 ± 0.2. The pH dependence of the rate of disappearance of the second intermediate (T_2) formed upon reaction with superoxide with reduced wt Nlr (k_3 in Scheme 2) is shown for comparison (○). The inset shows the pH dependence of the absorbance at 720 nm of the initial transient formed upon oxidation of wt Nlr with hexachloroiridate; the solid line assumes a single protonation equilibrium, with a pK_a of 6.2 ± 0.4.

Effect of Phosphate on the Reaction with Superoxide. Since studies of the E12 mutants in the presence of phosphate reveal spectral changes, the kinetics of O_2^- reduction was investigated in the presence of phosphate. The spectra of the species formed upon the reaction of superoxide with reduced E12V Nlr in the presence of 10 mM phosphate at pH 7.5 are depicted in Figure 6. The same initial transient (T_1) is obtained at the same rate as in the absence of phosphate, but the spectrum of the final species is distinct from that obtained in the absence of phosphate at the same pH. Instead, the final species absorbs at the same wavelength as K_2IrCl_6-oxidized E12V Nlr in the presence of phosphate (Figure 1C). This demonstrates that phosphate is bound to the protein upon formation of the final product.

When reduced wt Nlr is oxidized by O_2^- in the presence of phosphate, three distinct transient species are sequentially formed before the formation of the final 660 nm ferric species, instead of the two observed in the absence of

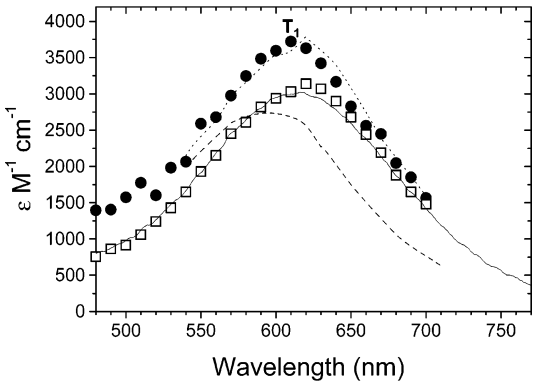

FIGURE 6: Transient visible absorption spectra formed upon reaction of E12V Nlr with O_2^- at pH 7.5 in the presence of 10 mM phosphate. Black circles depict the spectrum of the initial transient and white squares the spectrum of the final product. Dotted and dashed lines are the absorption spectra of the initial transient and final species, respectively, obtained in the absence of phosphate at pH 7.5 (as in Figure 2B). Air-saturated solutions contained 50 μM SOR, 2 mM Tris-HCl, 5 mM NaCl, 0.5 M ethanol, and 1.1−3.6 μM O_2^-. The solid line is the absorption spectrum of the oxidized enzyme at pH 7.5 in the presence of 10 mM phosphate.

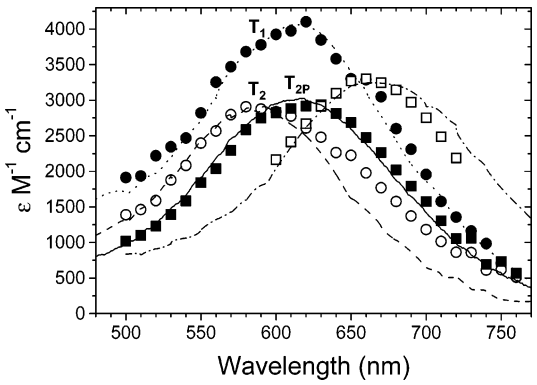

FIGURE 7: Transient visible absorption spectra formed upon reaction of wt Nlr with O_2^- at pH 7.5 in the presence of 10 mM phosphate. Black circles depict the spectrum of the initial transient (T_1), white circles that of the second transient (T_2), black squares that of the third transient (T_{2P}), and white squares that of the final product. Air-saturated solutions contained 50 μM SOR, 2 mM Tris-HCl, 5 mM NaCl, 0.5 M ethanol, and 1.1−3.6 μM O_2^-. Spectra of the transient species obtained in the absence of phosphate at pH 7.5 (as in Figure 2A) are shown for comparison: first transient (···), second transient (- - -), and final product (-·-). The solid line is the absorption spectrum of the oxidized E12V enzyme at pH 7.5 in the presence of 10 mM phosphate.

phosphate (Figure 7). Again, phosphate does not affect the rate of formation of the first transient (T_1) in wt Nlr, and its spectra, as well as that of the second transient, are virtually identical to those of the species formed in the absence of phosphate: T_1 and T_2, respectively. The spectrum of the additional third species (T_{2P}) is almost indistinguishable from that of the E12V final product obtained in the presence of phosphate at the same pH (the same intermediate species were observed at pH 6.5; not shown). This similarity suggests that T_{2P} observed in wt Nlr is a ferric Nlr where phosphate is bound to the iron center, as shown in Scheme 3.

As mentioned above, in E12V the T_1 species decays directly to produce the phosphate-bound form (T_{2P}), which is the final species. However, there is kinetic evidence of the formation of a second transient, as observed with the wild-type enzyme (T_2), but its spectrum, although

Scheme 3: Processes Observed during the Reaction of Reduced Nlr with $O_2\bullet-$ (after the formation of T_1) in the Presence of Phosphate

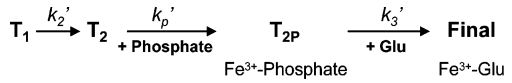

apparently shifted to blue with respect to the final product, was not significantly different from it (not shown). It is possible that the rate constants for the formation of T_2 and for its decay are not well separated in E12V, leading to the apparent immediate formation of the final product.

Both rates of decay of T_1 (k_2') and T_2 (k_P') obtained for wt Nlr are linearly dependent on phosphate concentration, at pH 6.5 and using a fixed concentration of NaCl (100 mM) (Figure 8A,B), indicating that phosphate is involved in both processes. Similar effects on the rate constants were obtained at pH 7.3 (not shown). In the E12V mutant, the rate of disappearance of T_1 also increases linearly with phosphate concentration. The existence of two phosphate-dependent steps in wild-type Nlr is intriguing, as only one vacant site on the iron is, in principle, available for binding. As the T_2 intermediate, assigned to a water-bound species, is still observed when phosphate is present, phosphate likely only binds after the formation of this transient, and therefore, the binding process should correspond to the second phosphate-dependent step. The role of phosphate in the disappearance of the initial transient, T_1, must be other than binding to the iron center. Here, most probably, the phosphate is acting as an acid, donating protons for the formation of hydrogen peroxide. The final step (k_3'), assigned to binding of glutamate to the $Fe^{3+}-$phosphate center with the consequent displacement of phosphate, also occurs at a rate that varies with phosphate concentration (Figure 8C), showing a significant decrease, as expected if phosphate is competing with glutamate for the same binding site. A general mechanism that is compatible with these results appears in Scheme 4where T_{2P} is the phosphate-bound transient and P is the concentration of phosphate. As P is in large excess, we can write $k_2''P = k_2'$ and $k_pP = k_p'$. Form the mechanism of Scheme 4, it is possible to derive expressions to fit the experimental data for the dependence of the rate constants on phosphate concentration (Figure 8; see the Appendix). In Table 2, calculated rates for the phosphate-dependent processes are given.

The equilibrium dissociation constant of phosphate at pH 6.5 can be estimated by a k_{-p}/k_p ratio of $\approx 4 \pm 1$ mM, which is close to the value previously determined from the saturation curve for the binding of phosphate to the E12V mutant at the same pH ($K_D = 3.6 \pm 0.1$ mM), and that should be similar for the wild-type protein.

Given the interference of phosphate in the reaction kinetics, the effect of formate was also tested. This was achieved by repeating the experiments at different pH values using ethanol as a $^{\bullet}OH$ scavenger instead of formate. The use of 0.5 M ethanol has no effect on the stability of any proteins studied in this work. No difference was observed with regard to the species formed or the rate constants, in the case of wt Nlr or the E12V mutant. This shows that the transient species observed here are not artifacts due to the presence of this radical scavenger.

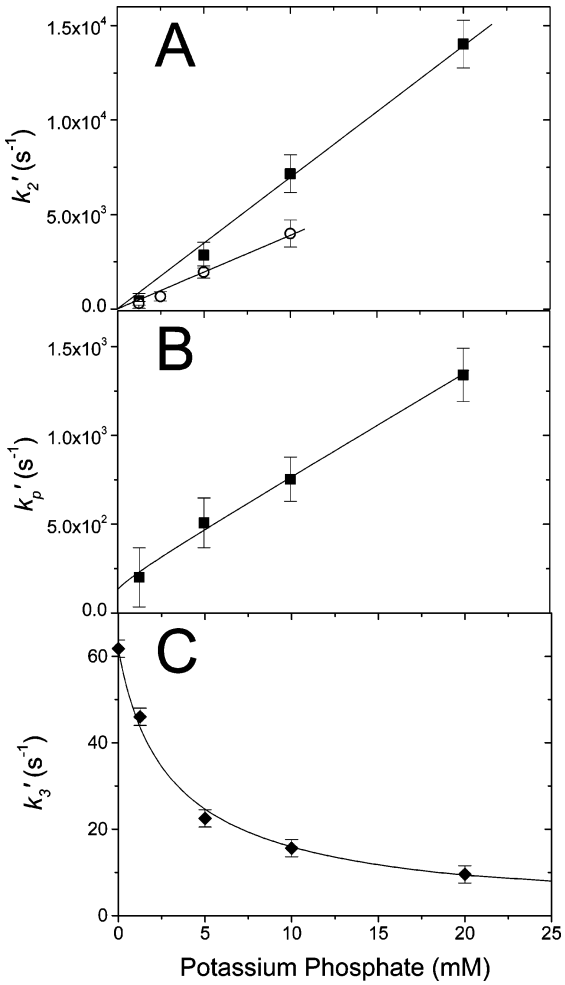

FIGURE 8: Dependence of rate constants (A) k_2', (B) k_p', and (C) k_3' (as in Scheme 3) on potassium phosphate concentration at pH 6.5 measured during the reaction of O_2^- with reduced wt Nlr (■) and E12V Nlr (○, A only). Solutions contained 50−100 μM SOR sites, 1.6 mM Tris-HCl, 0.5 M ethanol, 100 mM NaCl, and 50 mM NaCl for wt Nlr and the E12V mutant. Data points of k_2' were fitted with linear equations with slopes of 6.9×10^5 and 3.9×10^5 M^{-1} s^{-1}, for wt Nlr and E12V, respectively, after the value of k_2 in the absence of phosphate had been substracted (A). The solid line in panel B represents the best fit of the equation for λ_2 (see eq 11 of the Appendix) to the data points, with the following parameters: $k_p = 5.8 \times 10^4$ M^{-1} s^{-1} and $k_{-p} = 1.2 \times 10^2$ s^{-1}. The solid line in panel C represents the best fit of the equation for λ_3 (see eq 12 of the Appendix) to the data points, with the following parameters: $k_p = 5.8 \times 10^4$ M^{-1} s^{-1} and $k_{-p} = 2.1 \times 10^2$ s^{-1}. Values were averaged from three to five determinations, and the 95% confidence error intervals are reported.

Scheme 4: Proposed Mechanism for the Phosphate-Dependent Processes Occurring after the Formation of T_1

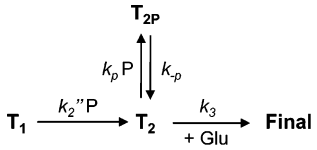

DISCUSSION

The equilibrium and fast kinetics data here obtained for *A. fulgidus* neelaredoxin and mutants (upon oxidation with substrate, superoxide, or a chemical oxidant, K_2IrCl_6) allow

Table 2: k_2'', k_p, and k_{-p} Rates Obtained for the Phosphate-Dependent Processes Observed during the Reaction of SORs with Superoxide[a] at pH 6.5

	k_2'' ($\times 10^{-5}$ M^{-1} s^{-1})	k_p ($\times 10^{-4}$ M^{-1} s^{-1})	k_{-p} ($\times 10^{-2}$ s^{-1})
Nlr	7 ± 1	6 ± 1[b]	2.1 ± 0.4[c]
E12V	4 ± 0.5	–	–

[a] The reaction mixture contained 50−100 μM SOR sites, 1.6 mM Tris-HCl, 0.5 M ethanol, and a fixed NaCl concentration of 100 or 50 mM for wt Nlr or the E12V mutant, respectively. The concentration of phosphate was varied from 1.25 to 20 mM (10 mM in the case of the E12V mutant). The 95% confidence intervals are reported. [b] Determined by fitting the equation for λ_2 (see eq 11 of the Appendix) to the data of Figure 8B. [c] Determined by fitting the equation for λ_3 (see eq 12 of the Appendix) to the data of Figure 8C.

a detailed characterization of the pH-dependent steps of the superoxide reduction and allow us to propose a general mechanism for this process.

pH-Induced Spectral Changes. The pH equilibria of wt and mutated (E12Q and E12V) Nlr suggest that a single protonation event modulates their spectral characteristics. The blue shift transition observed at high pH appears to be a common feature of SORs, as it was observed in all pH studies reported so far (*14*, *22*, *34*, *36*). The origin of this effect was recently identified as binding of hydroxide to the oxidized iron center, based on resonance Raman spectroscopy (*35*). Our following observations are consistent with this assignment. First, the high-pH species is very similar in neelaredoxin and both E12 mutants, while the low-pH form of the mutants exhibits lower extinction coefficients. This suggests that all three proteins share a common ligand at high pH, most probably a hydroxide. The difference observed at low pH for the E12 mutants in comparison with the wt protein is due to the fact that a water molecule is coordinating the ferric center instead of the glutamate ligand. Second, although phosphate addition results in spectral changes in the mutated proteins at acidic pH when compared to the wild-type enzyme, in the alkaline region no spectral differences are observed with regard to the presence or absence of this ligand. This suggests that hydroxide can bind and replace phosphate. Finally, the UV−visible spectra of Nlr and E12 mutants incubated with fluoride are very similar to the spectrum of the high-pH form, which supports the idea that binding of small anionic ligands, such as F^- and OH^-, can be responsible for the observed spectral changes. There is also strong kinetic evidence of hydroxide binding, which will be discussed below.

Reaction of SOR with Superoxide. The results allow us to propose a mechanism for O_2^- reduction by SOR (Figure 9). The kinetics obtained for the reaction of reduced Nlr with O_2^- suggest that two transient species are sequentially formed, each of them having a distinct electronic spectrum. Pulse radiolysis studies of Dfx from *D. vulgaris* and *D. baarsi*, as well as of Nlr from *T. pallidum*, also showed some evidence of the presence of two intermediates, but only in the last two cases were different spectral species obtained (*10*, *14*, *15*).

The first intermediate (T_1) is fully formed with a bimolecular rate constant of $\sim 10^9$ M^{-1} s^{-1}, having an absorption maximum at 620 nm. The formation of the T_1 intermediate is significantly slower in the E12V mutant. We have previously proposed, on the basis of molecular modeling

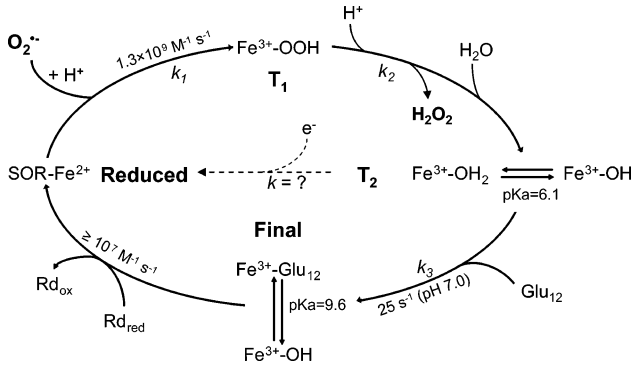

FIGURE 9: Proposed mechanism for the catalytic cycle of superoxide reduction by *A. fulgidus* neelaredoxin in vitro in the absence of buffer components. The k_2 rates are presented in the Results.

studies for the structure of *A. fulgidus* Nlr, that the glutamate residue is held in its position in the reduced form of the enzyme by two hydrogen bonding interactions with a histidine iron ligand, resulting in a conformation that leaves the active site groove open (*7*). The lower activity of the E12V mutant could be due the lack of capacity of valine to form hydrogen bonds, leading to a conformation that may lead to steric hindrance for the access of the substrate to the active site. Of course, this can certainly be in addition to or synergistic with a change in the electrostatic charge at the active site channel leading to a lower rate constant (*7*, *10*). The rate constant for T_1 formation in both *A. fulgidus* Nlr and the E12V mutant shows little pH dependence, which is analogous to the situation with *D. vulgaris* and *D. baarsi* Dfx (*10*, *14*). This can be interpreted as a lack of involvement of protons in this step or as the existence of a non-rate-limiting protonation; i.e., protonation occurs with a rate that has to exceed the observed rate of formation of T_1. In the first case, T_1 is most reasonably assigned to an iron-bound peroxo adduct, whereas in the latter, this adduct should be protonated. The disappearance of T_1 leads to the formation of a species that is common to the E12 mutants and wt Nlr, corresponding to the final product in the glutamate-free mutants. The spectral similarities between T_2, obtained upon oxidation of Nlr by superoxide, and the oxidized mutants, and a similarly low pK_a, led us to assign this transient to a water/hydroxide-bound ferric species. The subsequent process observed upon oxidation of wt Nlr must then correspond to the binding of glutamate. Fully consistent with this mechanism is the observation that the same transient (T_2) is formed if K_2IrCl_6 is used as oxidant instead of O_2^-, as observed by our stopped-flow experiments with wt Nlr, and decays to the final product at a rate similar to that obtained in the reaction with O_2^-.

These observations imply that hydrogen peroxide has already been released by the formation of the second species (T_2) and that the only "peroxo" adduct observed in our pulse radiolysis experiments is the T_1 species. Its decay (k_2) shows, for the wt protein, a pH-dependent decrease with an increase in pH when the pH is less than ~7, compatible with a rate-limiting protonation. A decrease in the rate constant for the decay of T_1 with an increase in pH was also observed for Dfx from *D. baarsi* and *D. vulgaris* (*10*, *14*). As the decay of T_1 is the only step that is demonstrably associated with the transfer of protons, due to its pH dependence (k_1 is essentially pH-independent) and the considerable solvent D_2O

effect observed in the case of *D.vulgaris* Dfx (*10*), and two protons are required for the formation of H_2O_2, the other protonation process should be nonlimiting. We expect that protonation of a doubly negatively charged iron−peroxo ($Fe^{3+}-O_2^{2-}$) adduct is much faster in comparison with protonation of an iron−hydroperoxo ($Fe^{3+}-HO_2^-$) adduct. Hence, we propose that the disappearance of T_1 involves the second protonation process which promotes the displacement of the hydroperoxo intermediate adduct from the iron center as H_2O_2, with immediate replacement by a water molecule, and that the T_1 intermediate must already be an $Fe^{3+}-HO_2^-$ species with the first protonation occurring immediately upon the reaction of superoxide with reduced SOR. Interestingly, the formation of the hydroperoxide intermediate was demonstrated for a biomimetic model of SOR, $\{Fe^{2+}[S^{Met}N_4(tren)]\}^+$, upon reaction with superoxide in methanol (*23*).

The proton donor responsible for the decay of T_1 has not been clearly identified. The kinetic data for k_2 in wild-type Nlr at low pH show a pH-dependent decrease with a slope ($\alpha = -0.35$) much lower than -1, the expected value for H_3O^+-mediated protonation. This contrasts with the pH profile of k_2 observed for Dfx from *D. vulgaris* and *D. baarsi*, where a much more pronounced slope was obtained, suggesting that protons arise from bulk solvent. By assuming such a process and fitting a linear equation with a slope of -1 to the data, we estimated the value for the second-order rate constant to be 10^8-10^9 M^{-1} s^{-1}. This value corresponds to a nearly diffusion limited protonation by H_3O^+ and is similar to those obtained in the case of Dfx from *D. vulgaris* and *D. baarsi*. The glutamate residue may be involved in this protonation step at low pH since, when it is mutated to valine or glutamine, loss of "peroxide" is slower and pH-independent at pH <7, in contrast with the case for the wild-type enzyme. In Dfx from *D. vulgaris*, the rate of disappearance of T_1 is higher in wt Dfx at pH <7 than in E47A Dfx, i.e., when the glutamate was mutated to alanine, compatible with a possible role for glutamate in the protonation of the bound peroxo moiety in this system (*10*). If one fits a single-protonation equilibrium equation to the data for the pH dependence of k_2, a pK_a of ≤5.7 is obtained. This could be attributed to glutamate, although it seems to be high for a solvent-exposed glutamate (the pK_a of free glutamate is ca. 4.5). Nevertheless, the specific environment surrounding this residue can significantly alter its pK_a; pK_a's as high as 6.7 have been measured for glutamate residues in proteins (*37*). Alternatively, the different pH dependence profiles observed in the E12 mutants in comparison with the wild type could simply reflect structural changes that affect the proton donation from bulk solvent or a specifically bound water molecule establishing a H-bond with nearby residues. In fact, the ∼2-fold higher value of k_2 observed for the E12Q mutant in comparison with that of E12V may be due to the hydrophilicity of glutamine that promotes protonation by water. A H-bonding network through water molecules was modeled in the recent structure of *T. pallidum* Nlr, interacting with the conserved proximal lysine (K49) (*38*). It has been proposed that lysine could be involved in proton donation to the peroxo species (*10*, *14*, *35*), probably via this H-bonding network. The presence of a lysine would certainly decrease the apparent pK_a of a nearby water molecule (*35*), thus constituting a source of protons for the nascent hydroperoxide. In this case, it is not surprising that mutation of the glutamate, which is next to lysine in the flexible loop, would interfere with the H-bond network hindering the protonation process. At pH >8, rate constant k_2 increases with pH in both wild-type and E12V *A. fulgidus* Nlr, indicating that the reaction mechanism at basic pH is probably different. Since this pH profile is consistent with OH^- binding, we propose that, at high pH, OH^- competes with the bound hydroperoxide species, with the latter being protonated by the bulk solvent (H_2O_2 pK_a = 11.6). In contrast with this profile, in Dfx from *D. vulgaris*, k_2 is pH-independent at basic pH, which points to some mechanistic differences among these systems.

The final process observed in wild-type Nlr, but not in the E12 mutants, corresponds to binding of glutamate, which as a consequence increases the pK_a for the spectral transition from 6.1 to 9.6. This step has been long predicted to occur, as it is known by other techniques that glutamate binds to the oxidized state, although it was never directly observed in fast kinetic experiments. The rate constant for this process decreases with pH until it reaches a plateau. A similar profile is observed for both the rate of decay and the spectral shift of the first transient observed upon oxidation of Nlr by K_2IrCl_6, with an apparent pK_a similar to that of the pH-induced transition of the T_2 species. This is entirely expected, since the binding of glutamate to a hydroxide-bound ferric species should be less favorable than to a water-bound one.

Binding of Phosphate. Our results show that phosphate binds to the oxidized center of E12 Nlr mutants, leading to changes in their electronic properties. Binding in the vicinity of the iron ion is also plausible, although the overall effect of phosphate change on the electronic properties, rate, and pK_a's is more indicative of a direct binding. Ligation of phosphate to the iron ion is not very surprising, as the active center is highly solvent exposed and binding of ferrocyanide, a similar bulky ligand, has already been observed by EPR spectroscopy and X-ray crystallography (*17*, *34*). In our previous work, phosphate was used in the final purification step of the proteins, compromising our conclusions regarding spectral differences between mutants and the wild-type protein (*7*, *26*). We also show here that phosphate changes the kinetics of the reaction of reduced SOR with superoxide. As our previous pulse radiolysis studies were carried out in the presence of high phosphate concentrations (*7*) and this buffer was also used in similar experiments performed elsewhere (*11*, *13*−*15*), the mechanistic conclusion based on these experiments may need to be revised.

In the presence of phosphate, the final product of the reaction of reduced E12V Nlr with O_2^- is identified by its spectral features as a phosphate-bound ferric species. This spectrum is similar to that of the additional transient appearing in the reaction of O_2^- with reduced wild-type Nlr (T_{2P}), suggesting that phosphate binds at some stage during the reaction despite the presence of a glutamate. The presence of phosphate does not change the spectral characteristics of the first two transients (T_1 and T_2), suggesting that neither of these species contains a bound phosphate. Therefore, the initial ferric species with bound water or hydroxide (T_2) likely interacts with phosphate to produce this new, phosphate-bound ferric species. This mechanism is supported by the linear dependency of the process on the concentration of phosphate. The disappearance of the initial transient, T_1,

assigned to protonation of the hydroperoxo intermediate and its consequent release as hydrogen peroxide from the iron center, is also linearly dependent on phosphate. Phosphate can be acting as a general acid here, donating protons to the presumed solvent-exposed hydroperoxo adduct. Similarly, a rate-limiting proton donation from general acids present in the medium was reported for an iron superoxide dismutase (*39*).

The final process, ascribed to binding of the glutamate, is also affected by the presence of phosphate, as the rate at which it occurs slows significantly with an increase in phosphate concentration. The observed kinetics could be rationalized by rate equations derived from a mechanism in which phosphate competes with glutamate for the same binding site. Moreover, the value for the dissociation constant obtained from these analyses is identical to the one obtained from the saturation curve for phosphate binding with the E12V mutant, further supporting this mechanism.

Comparison with Other Proposed Mechanisms. In similar pulse radiolysis experiments performed for SORs from *D. baarsi* and *T. pallidum*, two transient species were detected (*14*, *15*). The authors proposed that the first intermediate is an iron-bound peroxo species that decays to form a hydroperoxo adduct. They further suggest that this second intermediate would be protonated to form hydrogen peroxide by an uncharacterized step, with a predicted rate constant of $<5\ s^{-1}$. Here we also observed two transients (T_1 and T_2); however, as already discussed, T_2 is not a peroxo- or hydroperoxo-bound intermediate but is a water-bound ferric species. The only iron-bound peroxo or hydroperoxo intermediate observed here is the initial transient, T_1, and all remaining transient species (one, or two if phosphate is present) are the ferric form of the enzyme with different ligands. In the case of *D. vulgaris* Dfx, the first transient decays directly to the final product; i.e., the $Fe^{3+}-OH/OH_2$ species seen in *A. fulgidus* Nlr does not appear to form. It is not clear, however, if this arises from a different mechanism or if the $Fe^{3+}-OH/OH_2$ species actually forms in those proteins but its rate of disappearance is very high. Interestingly, although the rate of decay of T_1 in *D. vulgaris* E47A is similar to that of the wild type, the spectrum of the final product in the mutant is different and resembles that of an $Fe^{3+}-OH$ species. This is compatible with the binding of glutamate being nonlimiting, resulting in the apparent direct formation of the final $Fe^{3+}-Glu$ species. In this regard, a possible explanation for the presumably lower rate for glutamate binding in Nlr from *A. fulgidus* could be related to the thermophilic origin of this enzyme. It is well-known that thermophilic enzymes are more rigid at low temperatures, which, in this case, may justify why T_2 is observed, since its lifetime will depend on a significant conformational modification, which eventually will be faster at higher temperatures. This point will be the subject of future studies.

SOR Catalytic Cycle. One important aspect of the proposed catalytic cycle for O_2^- reduction (Figure 9) is that the reaction with O_2^- is completed and the iron is in the oxidized state after the decay of the initial transient, which, at pH 7.2 and at the concentrations that were used, corresponds to 1−5 ms after the pulse of O_2^-. This implies that re-reduction of SOR by rubredoxin or other reductants can occur immediately at this point, bypassing the slow step of glutamate binding. Reduction of the initial ferric species, here identified as T_2, is observed if excess ascorbate is used to reduce the oxidized enzyme (as described in Experimental Procedures) in pulse radiolysis studies. Therefore, under in vivo turnover conditions, glutamate possibly never binds to the oxidized enzyme. Considering the rate constants obtained here, together with the rate for the reduction of Nlr by rubredoxin (*25*), and that the physiological concentrations of these proteins are in the micromolar range, the rate-determining step for the reduction of O_2^- in vivo is most probably the diffusion-limited encounter between O_2^- and reduced one-Fe SOR, as also proposed for two-Fe SOR (*13*). This once again demonstrates the efficiency of this antioxidant system, comparable to canonical SODs, and its importance to anaerobic organisms in their protection against transient exposure to oxidative stress.

CONCLUSIONS

In summary, we have shown in this work that the reduction of superoxide by Nlr involves the formation of a single transient, which we propose to be an iron-bound hydroperoxide, which immediately decays by a proton transfer step to form an iron-bound solvent species in acid−base equilibrium. All other processes that we observe are related to only ligand binding to the metal and not to O_2^- reduction. The final step in the wild-type enzyme corresponds to the slow binding of the glutamate sixth ligand to the oxidized iron, a process that may be bypassed during in vivo catalytic turnover of the enzyme.

ACKNOWLEDGMENT

We thank João Carita for the growth of batch cultures at the ITQB/IBET Fermentation Plant. Pulse radiolysis studies were carried at the Center for Radiation Chemical Research at Brookhaven National Laboratory, which is supported by the U.S. Department of Energy (DE-AC02-98CH10086).

APPENDIX

Deriving the expressions for the rate constants of the mechanism:

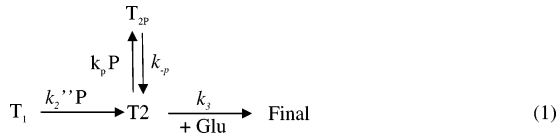

(1)

As P is in large excess, we can write $k_2''P = k_2'$ and $k_pP = k_p'$.

The differential rate equations for these processes are

$$\frac{dT_1}{dt} = -k_2'T_1 \quad (2)$$

$$\frac{dT_2}{dt} = k_2'T_1 - (k_p' + k_3)T_2 + k_{-p}T_{2P} \quad (3)$$

$$\frac{dTP}{dt} = - (k_p')T_2 - k_{-p}T_{2P} \quad (4)$$

A particular solution for the concentration variable of reagent X_i is

$$X_i = Ji e^{-\lambda t} \tag{5}$$

by substituting 5 into the previous equations (eqs 2−4):

$$-\lambda J_A e^{-\lambda t} = -k_2' J_A e^{-\lambda t} \tag{6}$$

$$-\lambda J_B e^{-\lambda t} = k_2' J_A e^{-\lambda t} - (k_p' + k_3) J_B e^{-\lambda t} + k_{-p} J_C e^{-\lambda t} \tag{7}$$

$$-\lambda J_C e^{-\lambda t} = k_p' J_B e^{-\lambda t} - k_{-p} J_C e^{-\lambda t} \tag{8}$$

The eigenvalues can be found by solving the determinant

$$\begin{vmatrix} \lambda - k_2' & 0 & 0 \\ k_2' & (\lambda - k_p' - k_3) & k_{-p} \\ 0 & k_p' & (\lambda - k_{-p}) \end{vmatrix} = 0 \tag{9}$$

$$\lambda_1 = k_2' \tag{10}$$

$$\lambda_2 = \frac{k_p' + k_3 + k_{-p} + \sqrt{(k_p' + k_3 + k_{-p})^2 - 4k_{-p}k_3}}{2} \tag{11}$$

$$\lambda_3 = \frac{k_p' + k_3 + k_{-p} - \sqrt{(k_p' + k_3 + k_{-p})^2 - 4k_{-p}k_3}}{2} \tag{12}$$

The general solution for each reagent X_i is constructed as a linear combination of the particular solutions (λ_1−λ_3):

$$X_i = J_{i1} e^{-\lambda_1 t} + J_{i2} e^{-\lambda_2 t} + J_{i3} e^{-\lambda_3 t} \tag{13}$$

where constants λ_1−λ_3 are the observed rate constants. Mechanism 1 can be rewritten as follows:

$$T_1 \xrightarrow{\lambda_1} T_2 \xrightarrow{\lambda_3} T_{2p} \xrightarrow{\lambda_3} \text{final}$$

The equations for λ_2 and λ_3 expressed as a function of phosphate concentration can be used to fit the data of panels B and C of Figure 8. The equation for λ_2 is mainly linear when $(k_p P + k_3 + k_{-p}) \gg 4k_{-p}k_3$ with a slope approaching k_p, and the intercept at the origin is equal to k_{-p}. Fitting this expression to the data of Figure 8B, one obtains $k_p = (6 \pm 1) \times 10^4\ M^{-1}\ s^{-1}$; the k_{-p} parameter could not be determined as it is affected by great uncertainty. Using the calculated value of k_p and fitting the expression of λ_3 to the data of Figure 8C, we obtain a k_{-p} value of $(2.1 \pm 0.4) \times 10^2\ s^{-1}$.

SUPPORTING INFORMATION AVAILABLE

Saturation plot for the binding of phosphate to the E12V mutant and absorbance versus time changes for the reaction of wt Nlr with superoxide in the absence and presence of phosphate. This material is available free of charge via the Internet at http://pubs.acs.org.

REFERENCES

1. McCord, J. M., and Fridovich, I. (1969) Superoxide Dismutase: An Enzymic Function for Erythrocuprein (Hemocuprein), *J. Biol. Chem. 244*, 6049−55.
2. Fridovich, I. (1995) Superoxide radical and superoxide dismutases, *Annu. Rev. Biochem. 64*, 97−112.
3. McCord, J. M. (2002) Superoxide dismutase in aging and disease: An overview, *Methods Enzymol. 349*, 331−41.
4. Jenney, F. E., Jr., Verhagen, M. F., Cui, X., and Adams, M. W. (1999) Anaerobic microbes: Oxygen detoxification without superoxide dismutase, *Science 286*, 306−9.
5. Lombard, M., Fontecave, M., Touati, D., and Niviere, V. (2000) Reaction of the desulfoferrodoxin from *Desulfoarculus baarsii* with superoxide anion. Evidence for a superoxide reductase activity, *J. Biol. Chem. 275*, 115−21.
6. Abreu, I. A., Saraiva, L. M., Carita, J., Huber, H., Stetter, K. O., Cabelli, D., and Teixeira, M. (2000) Oxygen detoxification in the strict anaerobic archaeon *Archaeoglobus fulgidus*: Superoxide scavenging by neelaredoxin, *Mol. Microbiol. 38*, 322−34.
7. Abreu, I. A., Saraiva, L. M., Soares, C. M., Teixeira, M., and Cabelli, D. E. (2001) The mechanism of superoxide scavenging by *Archaeoglobus fulgidus* neelaredoxin, *J. Biol. Chem. 276*, 38995−9001.
8. Jovanovic, T., Ascenso, C., Hazlett, K. R., Sikkink, R., Krebs, C., Litwiller, R., Benson, L. M., Moura, I., Moura, J. J., Radolf, J. D., Huynh, B. H., Naylor, S., and Rusnak, F. (2000) Neelaredoxin, an iron-binding protein from the syphilis spirochete, *Treponema pallidum*, is a superoxide reductase, *J. Biol. Chem. 275*, 28439−48.
9. Coulter, E. D., Emerson, J. P., Kurtz, D. M., Jr., and Cabelli, D. E. (2000) Superoxide Reactivity of Rubredoxin Oxidoreductase (Desulfoferrodoxin) from *Desulfovibrio vulgaris*: A Pulse Radiolysis Study, *J. Am. Chem. Soc. 122*, 11555−6.
10. Emerson, J. P., Coulter, E. D., Cabelli, D. E., Phillips, R. S., and Kurtz, D. M., Jr. (2002) Kinetics and mechanism of superoxide reduction by two-iron superoxide reductase from *Desulfovibrio vulgaris*, *Biochemistry 41*, 4348−57.
11. Lombard, M., Houee-Levin, C., Touati, D., Fontecave, M., and Niviere, V. (2001) Superoxide reductase from *Desulfoarculus baarsii*: Reaction mechanism and role of glutamate 47 and lysine 48 in catalysis, *Biochemistry 40*, 5032−40.
12. Emerson, J. P., Cabelli, D. E., and Kurtz, D. M., Jr. (2003) An engineered two-iron superoxide reductase lacking the [Fe(SCys)$_4$] site retains its catalytic properties in vitro and in vivo, *Proc. Natl. Acad. Sci. U.S.A. 100*, 3802−7.
13. Emerson, J. P., Coulter, E. D., Phillips, R. S., and Kurtz, D. M., Jr. (2003) Kinetics of the superoxide reductase catalytic cycle, *J. Biol. Chem. 278*, 39662−8.
14. Niviere, V., Asso, M., Weill, C. O., Lombard, M., Guigliarelli, B., Favaudon, V., and Houee-Levin, C. (2004) Superoxide reductase from *Desulfoarculus baarsii*: Identification of protonation steps in the enzymatic mechanism, *Biochemistry 43*, 808−18.
15. Niviere, V., Lombard, M., Fontecave, M., and Houee-Levin, C. (2001) Pulse radiolysis studies on superoxide reductase from *Treponema pallidum*, *FEBS Lett. 497*, 171−3.
16. Yeh, A. P., Hu, Y., Jenney, F. E., Jr., Adams, M. W., and Rees, D. C. (2000) Structures of the superoxide reductase from *Pyrococcus furiosus* in the oxidized and reduced states, *Biochemistry 39*, 2499−508.
17. Adam, V., Royant, A., Niviere, V., Molina-Heredia, F. P., and Bourgeois, D. (2004) Structure of superoxide reductase bound to ferrocyanide and active site expansion upon X-ray-induced photoreduction, *Structure 12*, 1729−40.
18. Coelho, A. V., Matias, P., Fulõp, V., Thompson, A., Gonzalez, A., and Carrondo, M. A. (1997) Dfx structure determined by MAD phasing and refinement to 1.9-angstrom resolution reveals a unique combination of a tetrahedral FeS4 centre with a square pyramidal FeSN4 centre, *J. Biol. Inorg. Chem. 2*, 680−9.
19. Lombard, M., Touati, D., Fontecave, M., and Niviere, V. (2000) Superoxide reductase as a unique defense system against superoxide stress in the microaerophile *Treponema pallidum*, *J. Biol. Chem. 275*, 27021−6.
20. Silaghi-Dumitrescu, R., Silaghi-Dumitrescu, I., Coulter, E. D., and Kurtz, D. M., Jr. (2003) Computational study of the non-heme iron active site in superoxide reductase and its reaction with superoxide, *Inorg. Chem. 42*, 446−56.
21. Horner, O., Mouesca, J. M., Oddou, J. L., Jeandey, C., Niviere, V., Mattioli, T. A., Mathe, C., Fontecave, M., Maldivi, P., Bonville, P., Halfen, J. A., and Latour, J. M. (2004) Mossbauer characterization of an unusual high-spin side-on peroxo-Fe^{3+} species in the active site of superoxide reductase from *Desulfoarculus baarsii*. Density functional calculations on related models, *Biochemistry 43*, 8815−25.
22. Mathe, C., Niviere, V., Houee-Levin, C., and Mattioli, T. A. (2006) Fe^{3+}-η_2-peroxo species in superoxide reductase from *Treponema*

pallidum. Comparison with *Desulfoarculus baarsii*, *Biophys. Chem. 119*, 38−48.
23. Shearer, J., Scarrow, R. C., and Kovacs, J. A. (2002) Synthetic models for the cysteinate-ligated non-heme iron enzyme superoxide reductase: Observation and structural characterization by XAS of an Fe(III)-OOH intermediate, *J. Am. Chem. Soc. 124*, 11709−17.
24. Theisen, R. M., and Kovacs, J. A. (2005) Role of protons in superoxide reduction by a superoxide reductase analogue, *Inorg. Chem. 44*, 1169−71.
25. Rodrigues, J. V., Abreu, I. A., Saraiva, L. M., and Teixeira, M. (2005) Rubredoxin acts as an electron donor for neelaredoxin in Archaeoglobus fulgidus, *Biochem. Biophys. Res. Commun. 329*, 1300−5.
26. Abreu, I. A., Xavier, A. V., LeGall, J., Cabelli, D. E., and Teixeira, M. (2002) Superoxide scavenging by neelaredoxin: Dismutation and reduction activities in anaerobes, *J. Biol. Inorg. Chem. 7*, 668−74.
27. Smith, P. K., Krohn, R. I., Hermanson, G. T., Mallia, A. K., Gartner, F. H., Provenzano, M. D., Fujimoto, E. K., Goeke, N. M., Olson, B. J., and Klenk, D. C. (1985) Measurement of protein using bicinchoninic acid, *Anal. Biochem. 150*, 76−85.
28. Fisher, D. S., and Price, D. C. (1964) Iron determination with TPTZ (tripyriyl-triazine: acid labile iron) in protein, *Clin. Chem. 10*, 21−31.
29. Gomes, C. M., Vicente, J. B., Wasserfallen, A., and Teixeira, M. (2000) Spectroscopic studies and characterization of a novel electron-transfer chain from *Escherichia coli* involving a flavorubredoxin and its flavoprotein reductase partner, *Biochemistry 39*, 16230−7.
30. Goto, J. J., Gralla, E. B., Valentine, J. S., and Cabelli, D. E. (1998) Reactions of hydrogen peroxide with familial amyotrophic lateral sclerosis mutant human copper−zinc superoxide dismutases studied by pulse radiolysis, *J. Biol. Chem. 273*, 30104−9.
31. Schwarz, H. A. (1981) Free radicals generated by radiolysis of aqueous solutions, *J. Chem. Educ. 58*, 101−5.
32. Buxton, G. V., Greenstock, C. L., Helman, W. P., and Ross, A. B. (1988) Critical Review of Rate Constants for Reactions Hydrated Electrons, Hydrogen Atoms and Hydroxyl Radicals in Aqueous Solution, *J. Phys. Chem. Ref. Data 17*, 676−80.
33. von Sonntag, C., and Schuchmann, H. P. (1991) The elucidation of peroxyl radical reactions in aqueous solution with the help of radiation-chemical methods, *Angew. Chem., Int. Ed. 30*, 1229−49.
34. Clay, M. D., Jenney, F. E., Jr., Hagedoorn, P. L., George, G. N., Adams, M. W., and Johnson, M. K. (2002) Spectroscopic studies of *Pyrococcus furiosus* superoxide reductase: Implications for active-site structures and the catalytic mechanism, *J. Am. Chem. Soc. 124*, 788−805.
35. Mathe, C., Niviere, V., and Mattioli, T. A. (2005) Fe^{3+}-Hydroxide Ligation in the Superoxide Reductase from *Desulfoarculus baarsii* Is Associated with pH Dependent Spectral Changes, *J. Am. Chem. Soc. 127*, 16436−41.
36. Chen, L., Sharma, P., Le Gall, J., Mariano, A. M., Teixeira, M., and Xavier, A. V. (1994) A blue non-heme iron protein from *Desulfovibrio gigas*, *Eur. J. Biochem. 226*, 613−8.
37. Chen, H. A., Pfuhl, M., McAlister, M. S., and Driscoll, P. C. (2000) Determination of pK_a values of carboxyl groups in the N-terminal domain of rat CD2: Anomalous pK_a of a glutamate on the ligand-binding surface, *Biochemistry 39*, 6814−24.
38. Santos-Silva, T., Trincao, J., Carvalho, A. L., Bonifacio, C., Auchere, F., Raleiras, P., Moura, I., Moura, J. J., and Romao, M. J. (2006) The first crystal structure of class III superoxide reductase from *Treponema pallidum*, *J. Biol. Inorg. Chem.* (in press).
39. Bull, C., and Fee, J. A. (1985) Steady-State Kinetic Studies of Superoxide Dismutases: Properties of the Iron Containing Protein from *Escherichia coli*, *J. Am. Chem. Soc. 107*, 3295−304.

BI052489K